Pairwise interactions between model swimmers at intermediate Reynolds numbers

Thomas Dombrowski, Hong Nguyen, and Daphne Klotsa

Pairwise interactions between model swimmers at intermediate Reynolds numbers

Thomas Dombrowski,[1] Hong Nguyen,[2] and Daphne Klotsa[2, *]

[1] *Department of Physics, The University of North Carolina at Chapel Hill, Chapel Hill, North Carolina 27599, USA*
[2] *Department of Applied Physical Sciences, The University of North*
Carolina at Chapel Hill, Chapel Hill, North Carolina 27599, USA
(Dated: June 12, 2022)

We computationally studied the pairwise hydrodynamic interactions for simple two-dimensional dimer model swimmers over a range of intermediate Reynolds numbers (Re) and for thousands of initial conditions, varying position and orientation. We found that the swimmers arranged in novel assemblies that were sensitive to initial conditions and Re. The resulting "phase diagrams" showed regions where the swimmers repel and swim away from one another, regions where they form stable pairs with different symmetries, and locations of transitions between them. The stable pairs fit neatly into combinations of five categories: swimmers in-line and side-by-side, parallel and anti-parallel, and perpendicular to one another. Once arranged into the preferred stable pair, the swimmers swam together or turned into a symmetric immotile pump, in both cases coordinating as one and generating combined fluid flows that stabilized the assembly. By looking at the pairs' steady state velocities, we were able to provide insight on possible benefits of being in a pair versus swimming alone. For some pairs, there seemed to be a clear speed advantage over the single swimmer, while for others the presence of a second swimmer slowed them both down. Moreover, we found that the stable pairs transition their swimming direction at different Reynolds numbers and when compared to the single swimmer. The time-averaged flow fields around each stable pair are also different from one another and from the single swimmer, and evolve as Re increases. Our results provide a guide for the complex nonlinear interactions that arise between self-propelled particles in fluids at intermediate Re by using the fluid inertia as a knob to control assembly behavior. They are the basis for scaling up towards many-body interactions and active matter of mesoscale swimmers.

PACS numbers: May be entered using the \pacs{#1} command.

I. INTRODUCTION

The collective behavior of organisms, such as swarms of bacteria and schools of fish, also known as active matter, has sparked the interest of many disciplines including physics, materials, biology, and engineering [1–9]. The nonequilibrium dynamic assemblies of swarms are distinct from equilibrium systems, in that, the constituent particles are motile and self-propelled – they convert their energy into motion. From a physics perspective, active-matter systems serve as a model for studying nonequilibrium ensembles theoretically [3, 5–7], but there are also numerous practical applications in materials [8], robotics [10, 11] and therapeutics [12]. The fluid medium, in which many swarms naturally occur, has been shown in many cases to play an important role in the underlying physical mechanisms and interactions that give rise to the collective behavior [13]. To make progress in active-matter theory and applications in fluids, we must have a better grasp of the fundamental physics of the hydrodynamic interactions for the simpler system of a pair of swimmers.

Before we discuss pairs, let us consider locomotion for a single swimmer as a function of length scale. In the microscopic world, locomotion is limited by the scallop theorem, which states that a swimmer with a reciprocal, time-reversible swim stroke cannot produce a net motion in Stokes flow [14]. Real organisms overcome the scallop theorem (break time reversibility) in one or combinations of at least three ways: i) with a non-reciprocal stroke, *e.g.* the corkscrew motion of the flagella of sperm cells and bacteria [15] or the three-sphere swimmer by Najafi and Golestanian [16]; ii) by swimming in groups or coordinating multiple appendages, *e.g.* microscopic cilia that beat together in a metachronal way [17, 18], and iii) by using inertial forces, *i.e.* their Reynolds number (Re = vL/ν), where usually the swimmer size L or velocity v or both are large enough for them to be in the intermediate (or high) Re regime [19, 20], *e.g.* fish larvae, brine shrimp and jellyfish [21, 22]. Note that the intermediate Re range is considered to be roughly between Re$_\text{int} \sim 1 – 1000$ [15, 23, 24]. Any one of these adaptations is sufficient to break time-reversibility, and many works have been dedicated to each. In reality, organisms developed not only to overcome the scallop theorem but also to be optimal and versatile in their swimming by combining (some or all of) the above mechanisms. For example, even though a bacterium performs a non-reciprocal stroke and can swim just fine in Stokes

flow, bacteria do swim in swarms and can achieve much higher swim speeds collectively than individually [4, 25–27]. Adult brine shrimp are large enough (∼cm size) to swim even with a reciprocal stroke, yet they evolved to use a nonreciprocal one, a metachronal wave of their limbs, which leads to more efficient swimming [28]. Numerical works on brineshrimp models that implement both the metachronal beating and the fluid inertia can been found here [29, 30]. From a fundamental physics and fluid dynamics point of view but also to impact applications in materials or robotics, there is no reason to constrain ourselves to one of these mechanisms; the system naturally provides different parameters that we can tweak to control pairwise and collective behavior. Thus, it is important to consider simple model systems combining these different mechanisms and to understand the physics at play. Here, we will be studying the effect of pair interactions between reciprocal swimmers, as fluid inertia is gradually introduced in the system, i.e. (ii) and (iii). We first discuss the interactions.

Numerous studies (both theoretical and experimental) have looked at the hydrodynamic interactions between either Stokesian swimmers at low Re [31–39] or purely inertial ones at high Re [40–46]. For example, sperm cells and B. Subtilis synchronize their flagella, and in doing so are hydrodynamically attracted to one another [31–33]. Many microscopic swimmers can be modeled as squirmers and then be classified as a "puller", "pusher", "neutral", etc. The puller has a force dipole, which induces a flow field that pulls in parallel to its swimming axis and pushes out in the perpendicular, while the pusher does the opposite. Puller pairs have been shown to attract along their swimming axis and repel in the perpendicular, and pushers have been shown to repel along the swimming axis and attract along the perpendicular, which has implications for example on how they swarm and accumulate near walls [15, 34, 35]. Collision dynamics for a model of chemically active droplets in Stokes flow were shown to be sensitive to the relative sizes of the droplets [36, 47]. Studies on the hydrodynamic interactions between a pair of dimer swimmers in Stokes flow have shown how the swimmers align and swim together, depending on their initial configuration [37–39]. The pair interactions between two asymmetric dimers in Stokes flow have been analytically solved for the one-dimensional case of reflection invariant pairs (collective swimming at a constant velocity) and translation invariant pairs (attractive or repulsive dependent on the leading swimmer orientation) [38]. A more extensive study derived stroke-averaged equations of motion for the effective hydrodynamic interactions between asymmetric dimer pairs in Stokes flow [39]. At the other limit, at high Re, where viscosity can be neglected, studies have been conducted on inertial swimmers modeled as vortex dipoles, flapping plates, and for specific organisms through computational fluid dynamics [40–46]. However, we have limited understanding in swimmer interactions at intermediate Re where both viscous and inertial forces coexist. Yet, the intermediate Re range is home to a plethora of biological organisms and particulate/robotic systems of interest.

A small number of studies have looked at the interactions between swimmers at the intermediate Re range [48–52]. Squirmers at intermediate Re and initially aligned in parallel will attract if they are pushers and repel if they are pullers [48]. When on a collision course, inertial effects change the contact time and scattering dynamics for pushers and can prompt hydrodynamic attraction and circular trapped trajectories for pullers [49]. The role of finite inertia on the collective behavior of swimmers beyond a pair remains largely unexplored, with the exception of Chatterjee *et al.* who identified stable, unstable and turbulent states for active suspensions of weakly inertial pushers [52] and Ouillon *et al.* [53] who reported increased diffusivity of swarms (compared to a single swimmer) and proposed a continuum model. Studies on biogenic mixing are related but the focus is more on the large-scale transport and mixing of the fluid that is generated by plankton and other mesoscale swimmers rather than the statistical mechanics of the swarms [54–58]. Apart from squirmers, the hydrodyanamic interactions for lattices of flapping plates at Re in the range (10-100) was studied recently [50, 51]. While squirmer and flapping-plate models have the advantage that they are well-understood mathematically, they are also quite specific and constrained in the assumptions that are being made. The squirmer model assumes a specific flow field that stems from low-Re swimmers, such as algae and bacteria and the amplitude of the surface oscillations, originally modeling beating cilia, is assumed to be small and cannot easily be varied. Real-life organisms and experimental systems will usually have finite or large amplitudes. On the other hand, flapping plates model a specific appendage geometry that is difficult to analytically solve [50] and, while they are common in nature, they are just one type of appendage. It is, thus, important to explore additional models that may offer new insights and an opportunity to identify universal behavior in the intermediate Re regime, where in nature there is an enormous diversity of motility mechanisms [59].

The dimer is a commonly-used model for swimmers, and has been extensively studied in Stokes, intermediate and inertial regimes for both Newtonian and viscoelatic fluids through theory, computer simulations and experiments [37–39, 60–70]. The dimer is a model swimmer composed of two equal or unequal spheres that either oscillate or rotate and are usually connected via a spring, rod, or adhere to a similar spatial constraint. In most works, and in our paper it is also a reciprocal swimmer. Its geometric simplicity has allowed analytical work and comparisons between theory, experiments and simulations. An additional advantage of most dimer swimmers is that they are mechanical models, in the sense that the swimmer generates its own flow field through oscillation, so no assumptions are made on the fluid field, which also means that one can directly study the effect of the amplitude of the oscillation (the stroke). We have shown, for example, that our dimer swimmer exhibits behavior seen in real life organisms, such as
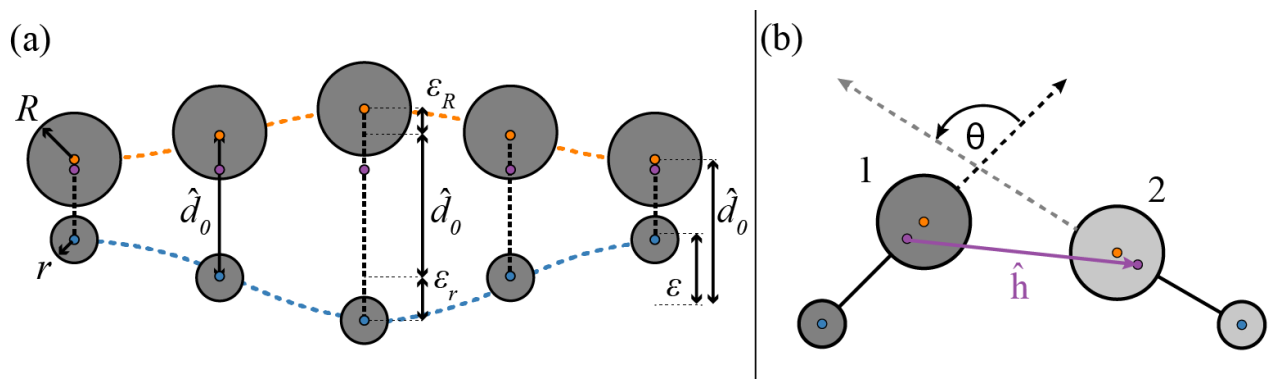
FIG. 1. (a) Swim stroke of the asymmetric dimer with sphere size ratio $\alpha = 0.5$. The dimer's large sphere (orange) oscillates in antiphase with the small sphere (blue) and the distance between them is prescribed to be of a simple harmonic oscillator with equilibrium length $\hat{d}_0$ and amplitude ε. (b) A pair of asymmetric dimers separated by a distance $\hat{h}$ and oriented with angle θ. θ is formed by the counter-clockwise rotation from the swimming axis of swimmer 1 to that of swimmer 2.

the back-and-forth motion during recovery and power strokes and a pusher-like or puller-like flow field for different parts of the oscillation [66, 71].

A question we asked in previous works was the following: how does a simple reciprocal swimmer, such as the dimer, go from rest to swimming as Re increases from zero to finite values? We showed that inertial effects in the fluid and specifically steady streaming flows can induce a transition from rest to motility going from Re = 0 to nonzero Re, and then a switch in the swimming direction from small-sphere leading to large-sphere leading [63, 66]. Hubert *et al.* [68] showed through experiments, theory, and computer simulations an interesting coasting effect due to phase lag that induces swimming for a dimer swimmer, in the special case where fluid inertia is zero but particle inertia is high. A related system with similar results was theoretically studied by Felderhof [61]. In another study, Collis *et al.* looked at an externally-vibrated dimer of unequal spheres in size and/or density at intermediate Re and did see a switch in swim direction, in their case generated by the coupling of translational and rotational motion due to the nonlinear convective body force [62]. Only recently, in Derr *et al.* [70] we studied the dimer analytically and numerically, and showed that it is important to make the distinction between fluid and particle inertia. The system is then quite sensitive to that balance of finite fluid and/or particle inertia and behaviors such as transitions in swim direction can vary. We expect that the forces at play will manifest even more in pairwise and many-body interactions, where nonlinear effects will add up giving rise to complex and surprising assemblies.

In this paper, we computationally studied the pairwise hydrodynamic interactions for reciprocal, asymmetric dimer model swimmers over a range of intermediate Reynolds numbers. Varying thousands of initial positions and orientations, we plotted "phase diagrams" showing regions where the swimmers repel and regions where they interact to form stable pairs. The stable pairs can be grouped as: in-line and side-by-side, parallel and anti-parallel, and perpendicular. Once formed, the swimmers in stable pairs were coordinated, swum together, and generated fluid flows as one. We studied the pairs' swimming velocities, separation distance, and their fluid flows as a function of the Reynolds number. We found that at low Re, in-line pairs are more frequent and act similar to a single swimmer (swim speed, direction, and fluid flow), while the side-by-side pairs become more frequent as Re increases and have more complex dynamics. The trend from in-line pairs at low Re to side-by-side pairs at high Re seems to be correlated to the time-averaged fluid flows around the pairs (steady streaming), which evolve and switch direction as Re increases. Overall, pair dynamics shows more complex behavior, different from the single swimmer, both in terms of swim speed and fluid flows as Re increases.

The structure of the paper is as follows. In section II, we describe the model, computational method, and simulation details. In section III we present our results starting with a review of single-swimmer behavior and expectations for pair interactions in (A), then the pair stable states formed by two asymmetric dimers in (B), and the pair dynamics and fluid flows for each stable pair as a function of the Reynolds number in (C). In section IV we summarize and discuss our conclusions.

II. MODEL AND METHODS

We consider a two-dimensional system of identical, asymmetric dimer swimmers. Each dimer is composed of two unequal sized spheres of radii R and r with an aspect ratio of $\alpha = r/R = 0.5$, see Fig 1a. The dimer's swimming axis

is along the line connecting the centers of the two spheres. The following conditions ensure that the dimer swimmer is force- and torque-free. The spheres are neutrally buoyant with respect to the surrounding fluid. The distance between the two spheres $\hat{d}(t)$ is prescribed to be of a simple harmonic oscillator such that $\hat{d}(t) = \hat{d}_0 + \varepsilon\sin(2\pi\tau)$, where $\hat{d}_0 = d_0/R = 2.5$ is the equilibrium distance between sphere centers, $\varepsilon = 0.8$ is the amplitude of oscillation, and $\tau = ft$ is the dimensionless time parameterized by f the frequency of oscillation. The amplitudes of each sphere are determined by the conservation of momentum $\varepsilon_r = \varepsilon R^2/(r^2 + R^2)$ and $\varepsilon_R = \varepsilon r^2/(r^2 + R^2)$, where subscripts R and r represent quantities specific to the large sphere and small sphere, respectively. Because $R = 2r$ we find that $\varepsilon_r = 4\varepsilon_R$. Note we non-dimensionalize our length scales by normalizing by the large sphere radius R.

The asymmetric dimer swimmers were immersed in a viscous, incompressible Newtonian fluid that occupied a finite cell with periodic boundary conditions. The fully-coupled fluid-structure interaction system was resolved using the Immersed Boundary (IB) method [72, 73]. The IB scheme was implemented in the open-source IBAMR software, which is an immersed boundary numerical method with adaptive mesh refinement [72]. The IB method for fluid-structure interaction uses an Eulerian formulation of the momentum equation and incompressibility constraint for the coupled fluid-solid system along with a Lagrangian description of the motion of the immersed structures. In previous works which focused on a single swimmer, we used a special case of IB within the IBAMR platform called the Constraint IB method (CIB) [74, 75]. CIB is faster and does not impose a constraint on the time step and spring stiffness. However, when introducing a second swimmer, we found that the hydrodynamic interactions due to the second swimmer led to additional torques that resulted in rotations of the individual spheres (rather than the swimmer as a whole). And, it was difficult to resolve collisions between swimmers. For these reasons, we used the standard IB method, in which the marker, spring system enabled us to easily prevent the individual spheres of each swimmer from rotating separately by tethering them together with inter-sphere springs so that they act as one rigid body and rotate about its center of mass. Standard IB also allows for a natural way to resolve collisions between swimmers as we will explain below. We describe our implementation of the standard IB method next.

Let $\mathbf{x} \in \Omega$ be fixed Eulerian physical coordinates, and let $\mathbf{s} \in U$ be fixed Lagrangian curvilinear coordinates attached to the structure, where Ω and U are the physical regions occupied by the fluid-structure system and structures respectively. In our notation, $\mathbf{X}(\mathbf{s}, t) \subset \Omega$ is the physical position of material point $\mathbf{s}$ at time t. The momentum equation and incompressibility constraint are given by

$$\rho\frac{D\mathbf{u}}{Dt}(\mathbf{x}, t) = -\nabla p(\mathbf{x}, t) + \mu\nabla^2\mathbf{u}(\mathbf{x}, t) + \mathbf{f}(\mathbf{x}, t), \tag{1}$$

$$\nabla \cdot \mathbf{u}(\mathbf{x}, t) = 0, \tag{2}$$

in which $\mathbf{u}(\mathbf{x}, t)$ is the Eulerian velocity field, $p(\mathbf{x}, t)$ is the pressure field that imposes the incompressibility constraint, $\mathbf{f}(\mathbf{x}, t)$ is a body force that arises from the presence of the immersed structure, ρ is the mass density, and μ is the viscosity. Eulerian and Lagrangian variables are coupled via integral transforms with Dirac delta function kernels:

$$\mathbf{f}(\mathbf{x}, t) = \int_U \mathbf{F}(\mathbf{s}, t)\,\delta(\mathbf{x} - \mathbf{X}(\mathbf{s}, t))\,\mathrm{d}\mathbf{s}, \tag{3}$$

$$\mathbf{U}(\mathbf{s}, t) = \int_\Omega \mathbf{u}(\mathbf{x}, t)\,\delta(\mathbf{x} - \mathbf{X}(\mathbf{s}, t))\,\mathrm{d}\mathbf{x}. \tag{4}$$

Eq. (3) converts the Lagrangian force density $\mathbf{F}(\mathbf{s}, t)$ to an equivalent Eulerian force density $\mathbf{f}(\mathbf{x}, t)$, and Eq. (4) evaluates the local material velocity at each structural position.

In our computer model, each sphere of the dimer was discretized using a collection of Lagrangian marker points that were generated using an in-house Python code, and the singular delta function kernels were replaced by a four-point regularized kernel function [72]. To maintain each sphere's rigidity, each marker point was connected with their nearest neighbors via intra-sphere stiff springs. The spheres were also connected by a set of inter-sphere springs which controlled their swim stroke oscillation and prevented individual sphere rotation. The force $\mathbf{F}(\mathbf{s}, t)$ applied on marker point $\mathbf{s}$ at time t was solely due to the linear expansion/compression of the springs. The spring force for marker points $\mathbf{s}_1$ and $\mathbf{s}_2$ connected by the spring ℓ was given by:

$$\mathbf{F}^\ell(\mathbf{s}_1, \mathbf{s}_2, t) = -K_s(|\mathbf{X}(\mathbf{s}_1, t) - \mathbf{X}(\mathbf{s}_2, t)| - R_\ell) \tag{5}$$

where K_s was the spring stiffness coefficient and R_ℓ was the resting length of spring ℓ. We note that $\mathbf{F}^\ell(\mathbf{s}_1, \mathbf{s}_2, t) = -\mathbf{F}^\ell(\mathbf{s}_2, \mathbf{s}_1, t)$. The resting length of the inter-sphere springs updates to the prescribed distance between $\mathbf{s}_1$ and $\mathbf{s}_2$ at every time step, while the resting length for the intra-sphere springs is kept fixed. For the inter-sphere springs, $K_s = 1.0 \times 10^4 \text{N/m}$, and for the intra-sphere springs, $K_s = 5.0 \times 10^4 \text{N/m}$. These stiffness coefficients have been chosen small enough for numerical stability, large enough to ensure that the individual sphere's deformation is negligible, and that the distance between spheres is approximately kept at the prescribed distance at all times. More details on the spatial discretization and the time stepping algorithm for the IB method can be found in references [72, 73].

TABLE 1. Dimensionless constants and variables in terms of R

Constant	Value	Definition
$\alpha = r/R$	0.5	aspect ratio of sphere radii for a single swimmer
ε	0.8	total amplitude of swimmer oscillation
ε_r	0.64	amplitude of small sphere oscillation
ε_R	0.16	amplitude of large sphere oscillation
$\hat{d}_0$	2.5	equilibrium distance between sphere centers
Variable	**Value range**	**Definition**
$\tau = ft$	[0,600]	time
$\hat{d}(\tau)$	$\hat{d}_0 + \varepsilon\sin(2\pi\tau)$	distance between sphere centers
$M^2 = R^2/\delta^2$	[6.4x10^{-3}, 0.64]	kinematic viscosity of the fluid
Re $= \alpha\varepsilon_r M^2$	[0.5,50.0]	Reynolds number of a single swimmer and its range
$\hat{h}(\tau)$	$\langle h_x(\tau), h_y(\tau)\rangle$	separation distance between dimers' center of mass
$\hat{h}(\tau = 0)$	$\langle \hat{H}_x, \hat{H}_y\rangle$	initial separation distance
$\hat{H}_x$	[0.0,6.25]	range of initial x-separation distance
$\hat{H}_y$	[-4.5,4.5]	range of initial y-separation distance
θ	[0.0,337.5]	angle in degrees between two swimmers

In IBAMR, an adaptive fluid grid is implemented to improve the efficiency of the simulation. There were four refinement levels (N=16, 64, 256, and 1024). In previous work we did a refinement study (see Supplemental Information in [63]), where we showed that the highest refinement was both accurate and computationally feasible. So, the dimer meshes were evaluated at the highest grid refinement of N=1024 and grid spacing of $d\hat{X} = dX/R = L/NR = 0.049$, where L is the size of the simulation box. The spacing between marker points is set by the standard IB method to be $d\hat{S} = 0.5d\hat{X}$ to avoid fluid leak into the spheres. The size of the simulation box, $L = 12.5(d_0 + R + r) = 50R$, was large enough, such that the velocity of a single swimmer and of the pairs decayed to zero before reaching the simulation boundary, see Supplemental Information (SI) section I [76]. We thus expect finite size effects to be negligible. Close contact between immersed structures are automatically handled by IBAMR with an enhanced version of the kernel function [77]. Therefore, no special treatment is needed for the collision between dimers within the IB scheme currently employed.

The pair system was composed of two identical dimers parameterized by the separation distance at time t, $\hat{h}(t) = h(t)/R$ between the dimers' centers of mass, and the counter-clockwise angle formed between their swimming axes θ, see Fig. 1b. The initial conditions are stated as $\hat{h}(t = 0) = \hat{H} = \langle \hat{H}_x, \hat{H}_y\rangle$ We used the frequency Reynolds number of the small sphere Re $= \alpha\varepsilon_r M^2$, with viscosity $M^2 = R^2/\delta^2$ and boundary layer thickness $\delta = \sqrt{\nu/\omega}$. The reason for the choice of Re is that it has been found to control the transition of swimming dynamics in the single dimer system [63, 66]. Note that there are many Reynolds numbers (dimensionless ratios) that can be defined because of the many relevant length scales (e.g. the spheres' two radii, amplitude, distance between spheres etc.) – for a discussion see Dombrowski *et al.* [66]. We monitored the swimming pair until the swimmers either diverged ($\hat{h} > 10$) or reached a steady state (separation distance $\hat{h}$ and angle θ changed by less than one percent over consecutive swim strokes). We monitored the pairs until steady state had been reached, and the simulation duration varied from at least twenty to six hundred oscillations. A note on 2D versus 3D. Our results here are all in 2D, but we know from previous works [63] that qualitatively (and quantitatively to a large extent) the behaviors we study and find in 2D for a single swimmer are the same as in 3D. We show the velocity curve as a function of Re for a 3D swimmer in the SI, section II [76]. Of course, the fluid flows are more complex in 3D, and the pairwise behavior may also change, but as an initial investigation, we focus on 2D.

III. RESULTS

A. Single swimmer

Before we describe the results for the pair interactions between swimmers, we summarize what we already know about the motility of a single swimmer at intermediate Re using the dimer model. The dimer model consists of two discs (or spheres) connected by a spring that oscillate with respect to each other. One important connection that we made in previous works [63, 66] was to steady streaming flows [78, 79]. Steady streaming is the nonzero time-averaged fluid flow generated by rigid bodies oscillating in a fluid at intermediate Re and has been studied analytically for specific geometries (e.g. spheres, discs, walls) and in specific regimes, where approximations can be made, such as
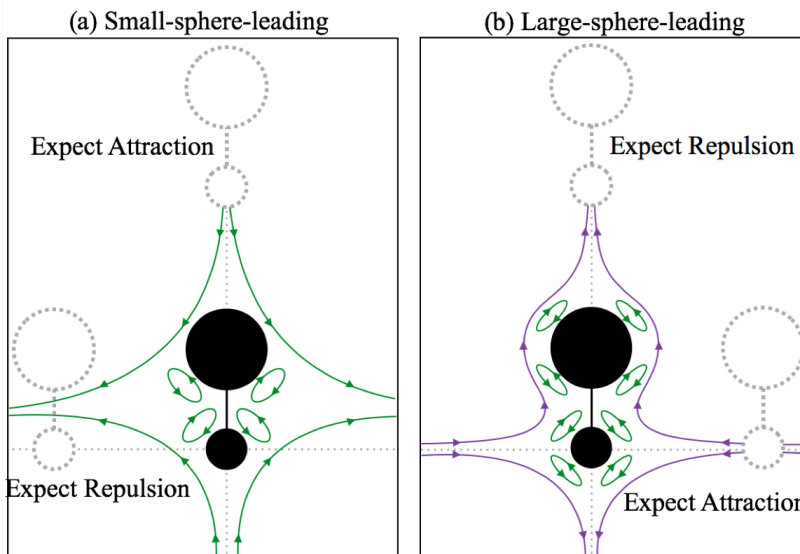
FIG. 2. Schematic of the averaged fluid flow around a single dimer swimmer in the a) small-sphere-leading and b) large-sphere-leading regime. Inner vortices (green) pull in the fluid along the swimming axis and push out perpendicular to it. The small-sphere-leading swimmer is puller-like. Secondary outer vortices (purple) seen in (b) do the opposite, push fluid away from swimming axis and pull in fluid perpendicular to it. The far field flow of the large-sphere-leading swimmer is pusher-like. We expect for a second dimer swimmer to attract along the pulling directions and repel along the pushing directions for both small-sphere-leading and large-sphere-leading swimmers.

small oscillation amplitude. Riley [79] showed that for one oscillating sphere there are two limiting cases to the time-averaged fluid flow, one when $\delta \gg r$ and the other when $\delta \ll r$, where δ is the oscillatory boundary layer thickness defined as $\delta = \sqrt{\frac{\nu}{\omega}}$ and r is the radius of the sphere. When $\delta \gg r$, the boundary layer is large and the average flow pulls in along the direction of oscillation and pushes out in the perpendicular. When $\delta \ll r$, the boundary layer is thin and confined near the surface of the sphere, and a secondary outer vortex develops where the far-field average flow is reversed, i.e. pushes out parallel to and pulls in perpendicular to the direction of oscillation, see Figs. 1,2 in Ref [79], and Fig.3(c)-(f) in Ref [63]. Previous studies have investigated steady streaming flows between pairs of cylinders or spheres [80, 81] and we have shown through experiments and simulations how they can lead to assemblies of granular systems [82, 83].

We found that the dimer swimmer, with two spheres oscillating in antiphase, generates similar steady streaming flows but with additional complexities. Specifically, the dimer swimmer also exhibits a reversal in its averaged flow field (much like the single oscillating sphere), but due to the swimmer's asymmetry, the reversal of flows corresponds to a transition in the swimming direction. For Re $\lesssim 18$ the flow field is puller-like, i.e. it pulls in along the swimming axis and pushes fluid out in the perpendicular, and the swimmer swims small-sphere-leading, see Fig. 2a. For Re $\gtrsim 18$, the flow field is pusher-like, i.e. it pushes fluid away along the swimming axis and pulls fluid in on the perpendicular, and the swimmer switches direction and swims with the large sphere on the front, see Fig. 2b and references [63, 66]. We should note that the reversal of the fluid flows is gradual. As Re increases, the inner circulation gets thinner (boundary layer thickness) and the outer recirculation vortices appear. We quantified the transitions in swimming direction and averaged fluid flow by collapsing the data to a critical transition Re that was ≈ 18 [63]. Our interpretation was that the small sphere dominates the motion because it has a relatively large amplitude, $\epsilon_r = 4\epsilon_R$, and it acts like an appendage while the large sphere is more like the swimmer's body. Thus when the small sphere is on average pulling fluid in towards the swimmer, it is pulled in that direction (of the small sphere). On the other hand, when the small sphere is on average pushing fluid away from the swimmer, the jet below the small sphere pushes it in the opposite direction (large-sphere leading). Note that the transition in the swim direction occurs at Re ≈ 18 using the CIB method as in [63, 66] and at Re ≈ 15 using the standard IB method in the current paper. We believe that the reason for the discrepancy is that in CIB the swimmer is constrained to move on a specific axis (there is no lateral motion or wobbling), while in IB this is not true. We have confirmed that the fluid flows and general trends are all the same.

Based on what we know for the single swimmer case, how do we expect two swimmers to interact? A simple hypothesis is that when the swimmers are puller-like they would attract along the pulling direction, i.e. along the swimming direction forming a line one behind the other, and that other configurations e.g. side-by-side would be unstable because the flow is pushing away, see Fig. 2a. On the other hand, when the swimmer is pusher-like, we might
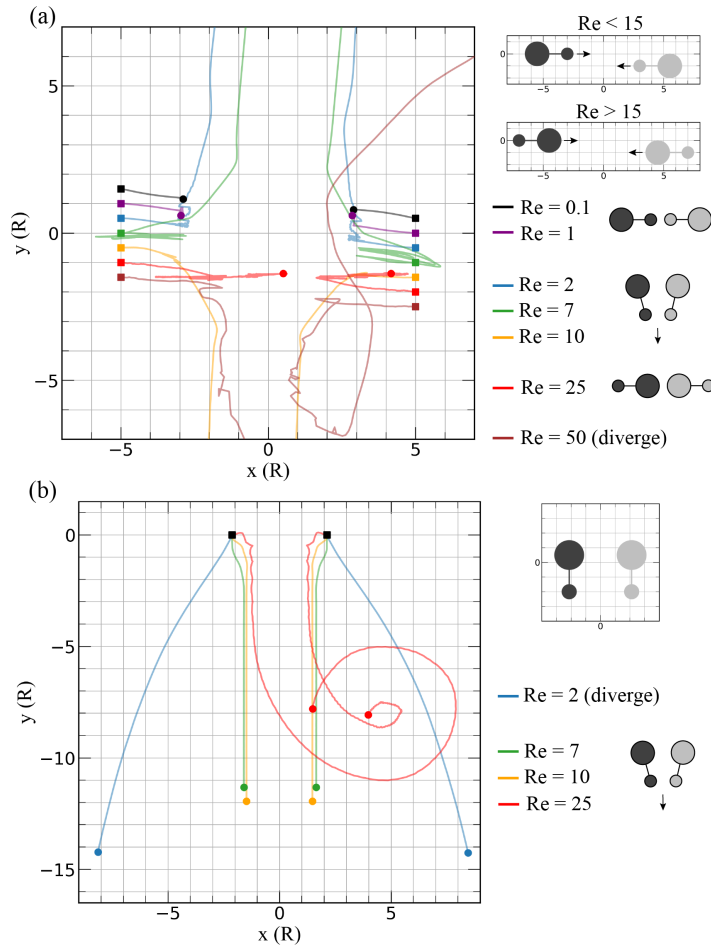
FIG. 3. Trajectories of two dimer swimmers at different Reynolds numbers, as they approach each other on a collision course in (a), and when they swim side-by-side in (b). Squares indicate initial positions and circles final positions. On the right of each trajectory plot, we show the initial arrangement at the top (collision course in (a) and side-by-side in (b)). Next to each Re we indicate the corresponding pair that forms with a schematic or note it diverges. The trajectories are offset by $dy = 0.5$ to display the information more clearly. The square scatters represent the initial configuration for each dimer, and trajectories are color coded by Re.

expect that a sideways arrangement would be more favorable, see Fig. 2b. In the next sections, we will show how this is a reasonable initial hypothesis but is not the full story. To get a better understanding, we can break things down to the following questions for each system: i) what is the swim direction of the stable pair? ii) Does it relate to the single swimmer's swimming direction? iii) what is the averaged fluid flow around the stable pair? iv) does it relate to the single swimmer's fluid flow? Comparing the swimming directions and fluid flows for the stable pairs amongst them and with the single swimmer will give us more insight.

B. Pairwise interactions of dimer swimmers

1. Dimers approaching each other

In this section, we consider the pairwise interactions of two dimer swimmers on a collision course and how they are affected by a gradual increase in inertia, similar to the study by Li *et al.* for inertial squirmers [49]. The dimers' centers of mass were initially offset by $\hat{H}_x = 10$ and $\hat{H}_y = 1$ at an angle of 180 degrees from one another. When Re < 15, the dimers were initially oriented with their small spheres closest such that they would swim toward each other. Otherwise, they were initially aligned with their large spheres closest due to the switch in swimming direction.

For all Reynolds numbers, we found that the swimmers quickly aligned their swim axes (which were initially offset).

When Re ≤ 1.0, the swimmers approached and got hydrodynamically trapped to form an antiparallel immotile pump with their small spheres closest, see Fig. 3(a). This in-line antiparallel pair is a stable configuration. Note that this is in contrast to the inertial pullers at similar Re, which rotate to avoid close contact and swim away from one another [49]. When $1.0 < \text{Re} \leq 10.0$, the swimmers' small spheres collide softly, and after a couple of collisions they rotate about 90 degrees to form a cooperative and stable side-by-side V-shape pair. The side-by-side V pair reaches a steady state and swims at a constant speed in the direction of the small spheres. We note that even though the angle of the V-pair is quite large here ($\approx 55^0$), it is surprising to see a stable pair in a side-by-side orientation when the individual dimers on their own exhibit puller-like flow (see Fig.2(a)).

When Re > 15.0, the dimer's individual swimming direction switches from small-sphere-leading to large-sphere-leading. (For that reason, we flip the initial orientations of the dimers to have their large spheres closest). At these Reynolds numbers, we see two types of behavior. At Re = 25.0, see red curve in Fig. 3(a), the swimmers approach, they collide into one another softly (their large spheres) but do not scatter away. Unlike the inertial squirmers which rotate out of the plane and eventually scatter, the two dimers block each other's swimming paths and are trapped in a loop of gentle collisions. As Re increases, the collisions are more energetic. Eventually the dimers collide and escape each other, see brown curve in Fig. 3(a).

2. *Dimers moving side-by-side*

We also consider the pair interactions for dimers initially moving side-by-side and how the behavior changes with Re. The dimers' centers of mass are initially at a horizontal distance $\hat{H}_x = 4.25$, and are initially parallel to one another ($\hat{H}_y = 0$) at an angle of 0 degrees, see schematic in Fig. 3(b) legend.

When Re = 2.0, the swimmers repel one another. They initially remain oriented in parallel in a side-by-side configuration where they swim at the same speed small-sphere-leading, but the distance between them increases as the simulation progresses. Eventually, they are two independently swimming dimers. At higher Re, see Re = 7.0, 10.0, 25.0 in Fig. 3(b), the swimmers are attracted to one another and reorient themselves to form a stable side-by-side V-shape, much like the one seen when they were initially on a collision course. Together, they swim in the direction of their small spheres. The separation distance and angle between the swimmers decreases as Re increases.

We see that V-pairs occur robustly from both initializations for Re = 7, and Re = 10. At lower Re, the side-by-side configuration where they are exactly parallel has the swimmers repel, which makes sense, while the collision course (that is offset) allows them to rearrange and form a stable V-pair. On the other hand at higher Re (Re = 25), the collision course does not allow the pair to form while the side-by-side works well to stabilize it. Some of the behavior observed when moving side-by-side is unexpected; for example, the dimers attract when placed side-by-side at Re = 7.0 and 10.0 leading to the V-pair. The single dimer swims small-sphere-leading and has an averaged flow field much like a puller. We expect that if the swimmers are placed side-by-side they would be repelled and swim away from one another. We further explore the parameter space of initial positions and orientations to develop a better understanding.

C. Emergent stable pairs as a function of initial conditions

We performed a large sweep (more than 6,000 simulations) over position and rotation space, varying the initial separation distance, $0.25 \leq \hat{H}_x \leq 6.25$ and $-6.5 \leq \hat{H}_y \leq 4.5$, over angles θ in the range $0 - 360$ degrees (increments of $360/16$) for four representative intermediate Reynolds numbers, Re = 2, 7, 10 and 25. Recall that a single swimmer switches direction at Re ≈ 15 so depending on the Re, the initial configurations are such that the swimmers either move towards each other or away from one another.

Depending on the initial positions, the swimmers either repelled and swum away from one another or assembled a stable pair. To form a stable pair, the swimmers first attracted or repelled (if too close), rearranging their separation and orientation until they "locked" into the preferred pair. Then the swimmers would swim together in a coordinated way as one unit. The large number of initial configurations simulated allowed us to formulate two surprising findings compared to inertial squirmers: i) that so many of the simulations led to stable pairs and ii) that the stable pairs can be quantitatively described by combinations of five simple arrangements as shown schematically in Fig. 4 (top): in-line (parallel and antiparallel), side-by-side (parallel and antiparallel), and perpendicular. Note that the details of the pairs vary with Re, *e.g.* the distance or exact angle between swimmers in a pair. A full breakdown of the conditions used to identify stable pairs is shown in the SI section III [76].

To quantify our results, we took 2D slices of the three-dimensional "phase diagrams" of the stable pairs as a function of the initial relative positions (in x and y) and angles between the swimmers. We show a slice at four characteristic Re, see Fig. 4. Specifically, the plots show the vertical distance $\hat{H}_y$ versus the angle θ between swimmers at fixed

horizontal distance $\hat{H}_x = 4.25$ (which captures a lot of the interesting behavior). Diagrams for all values of the horizontal distance $\hat{H}_x$ simulated are included in the SI section III [76].
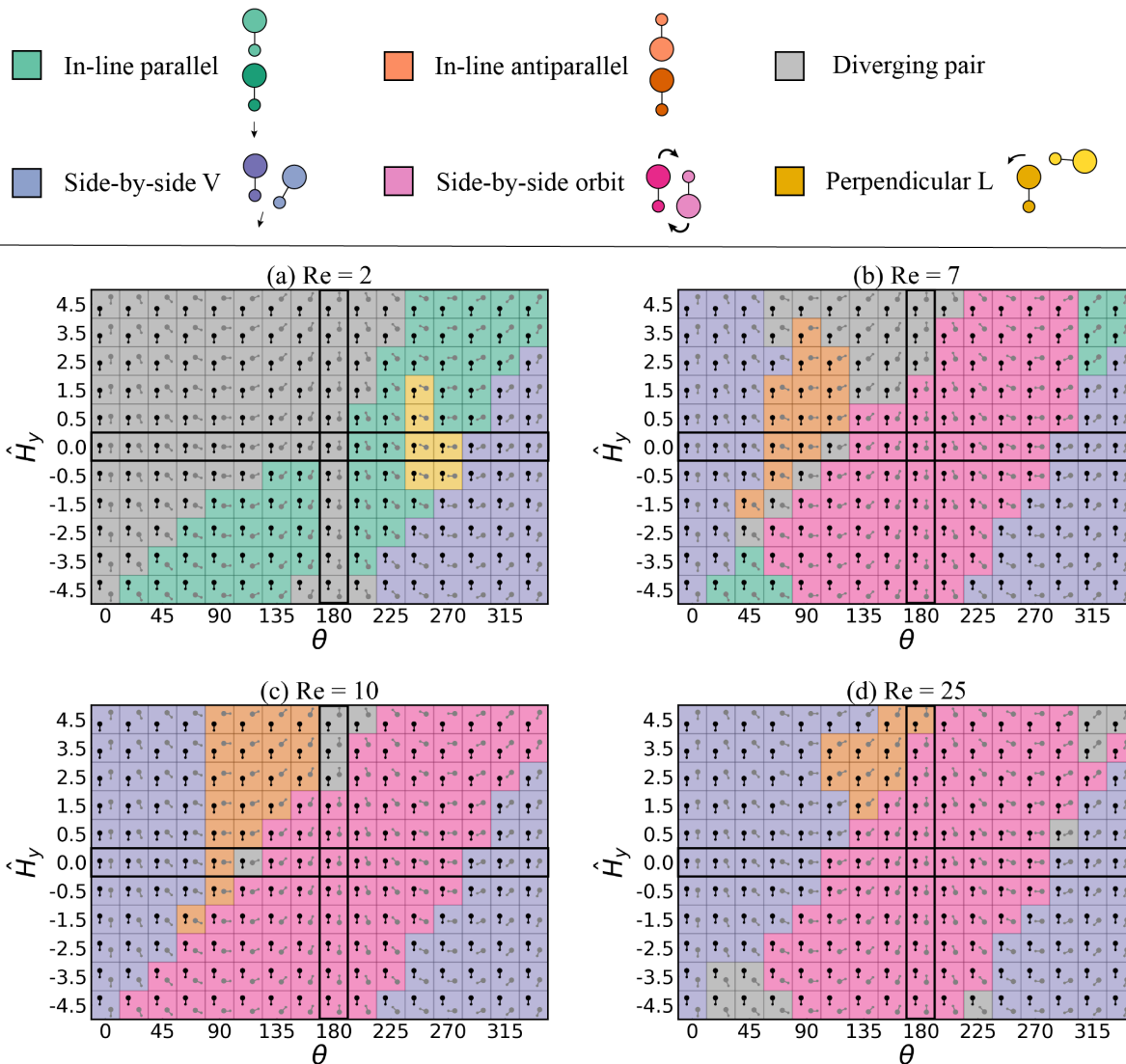

FIG. 4. Identified regions of diverging or stable pairs after steady state had been reached for (a) Re = 2, (b) Re = 7, (c) Re = 10, and (d) Re = 25 based on initial configurations $\hat{H}_y$ and θ for constant $\hat{H}_x = 4.25$. Initial configurations are determined based on the position and orientation of the grey swimmer with respect to the black swimmer. (Top) Schematic of pair behaviors and corresponding colors: in-line parallel (green), in-line antiparallel (orange), side-by-side V (blue), side-by-side orbit (pink), and perpendicular L (yellow). Pairs which were seen to diverge, $\hat{h} > 10$, are colored in grey.

Let us first consider Re = 2. When the swimmers are initially side by side *i.e.* $\hat{H}_y = 0$, we see that for angles between $0 - 180$ degrees the swimmers repel and diverge in swimming paths, see Fig.4. This makes sense if we look at the corresponding initial configurations and recall two things: that the flow field around each swimmer is puller-like (in towards the spheres along their swimming axis, and pushing away from the swimmer on the perpendicular) and that they swim in the direction of the small sphere. Thus we expect that sideways initial configurations would result in repelling swimmers (as we saw in previous section, Fig.3(b)). As the initial angle between the swimmers gets larger than 180, the swimmers are now off center, see for example ($\theta = 225°, \hat{H}_y = 0$) in Fig.4(a), and so the swimmers slightly rotate to form an in-line parallel pair. As the angle is close to perpendicular the swimmers form an L-shape and as the angle increases more, they discover another stable configuration that is a side-by-side V-shape pair. We should note that the V-pairs here have a large angle between them ($\approx 55°$). In both the parallel in-line and the V-shape pairs, the swimmers move together as a unit in the direction of the small spheres. The L-shape pairs also

swim as one, forming an arc trajectory, where the direction of the pair seems to be the same as the vector sum of the individual swimmers' velocities. When $\hat{H}_y$ increases in magnitude, the swimmers are off center and we see a lot of stable pairs when the swimmers are arranged such that they are swimming towards one another, i.e. when $\theta > 180°$. We also see a cluster of stable in-line parallel pairs that form when $\hat{H}_y < 0$ and $\theta < 180°$. We attribute this behavior to the attractive flow along the swimming axis. In all these cases, the black swimmer reorients itself to follow the grey swimmer in tow until they approach one another and form a stable in-line parallel pair (small-sphere leading).

As Re increases, for Re = 7 and 10, we see transitions and differences in pair behavior compared to Re = 2. Note that the dimers still individually swim small-sphere-leading, and the averaged fluid flow resembles a puller-like flow, see Fig.2(a). When the swimmers are initially side by side, $e.g.$ $\hat{H}_y = 0$, for angles between $0 - 45$ degrees they reorient to form a side-by-side V-pair, see Fig. 4(b,c). So, instead of swimming away from one another as they did for Re = 2 θ between $0 - 45°$, and $\hat{H}_y = 0$, here at Re = 7 they get trapped into a V-pair. The V-pair has an angle between the swimmers, $\theta_V = 32°$ for Re = 7 and $\theta_V = 29°$ for Re = 10, and separation distance, $\hat{h} = 3.3$ for Re = 7 and $\hat{h} = 3.0$ for Re = 10. Both the V-pair angle and the separation distance decrease as Re increases. This is expected as the boundary layer thickness goes down as Re increases and the swimmers can move closer. Let us focus on Re = 7 (Fig. 4(b)) but the same observations apply for Re = 10 (Fig. 4(c)). As the initial angle increases, the pair transitions from assembling into a side-by-side V to an in-line antiparallel pair, see for example $(\theta, \hat{H}_y = 90°, 0)$ in Fig. 4(b). The swimmers reorient from being initially perpendicular to one another to antiparallel with their large spheres closest. Each swimmer individually has a puller-like flow on average, which favors the in-line alignment but each swimmer also wants to swim with the small sphere on the front, which acts opposite to that attraction. It seems that for these in-line antiparallel pairs there is a competition between these two forces. The resulting pair is an immotile pump that oscillates in place but does not move – the swimmers are hydrodynamically trapped and do not escape. For larger initial angles, between $135° - 270°$, the swimmers assemble a stable side-by-side orbiting pair, where the swimmers are pointing in opposite directions. The dynamic pair orbits in the direction of the large spheres (clockwise in Fig. 4(b)) which is surprising, because the individual swimmers in isolation would swim in the direction of the small sphere. It is evident that there are many-body interactions not captured or predicted by the single-swimmer behavior. When $\theta > 270°$, the swimmers attract to form the side-by-side V-shape seen previously for small angles at Re = 2. When the swimmers are off center e.g. $\theta, \hat{H}_y = 45°, -4.5$, we also see some in-line parallel pairs, similarly to Re = 2.

Increasing the Re further, at Re = 25, almost all initial configurations lead to side-by-side stable pairs, see Fig. 4(d). This is somewhat expected from knowledge that for an individual swimmer the time-averaged flow field at higher Re is pusher-like, Fig. 2(b). When the swimmers are initially alongside one another i.e. $\hat{H}_y = 0$, we see the formation of side-by-side stable pairs depending on the angle. When the two swimmers are initially oriented such that they swim in the same vertical direction (e.g. for $(\theta, \hat{H}_y = 45°, 0)$ in Fig. 4(d)), they assemble into a side-by-side V pair with an even smaller angle, $\theta_V = 20°$, and separation distance, $\hat{h} = 2.5$. On the other hand, when the two swimmers are initially swimming in opposite directions (e.g. $(\theta, H_y = 180, 0)$ in Fig.4(d)), they reorient to antiparallel and attract to form a stable side-by-side orbit.

We observe similarities and differences in pair behavior across Re. The region of side-by-side V pairs for $\theta > 240°$ is seen for all Re studied, see bottom-right region of all panels in Fig. 4. The formation of stable side-by-side V pairs at Re $< 15°$ cannot be explained by the individual swimmer averaged flow which disfavors sideways pairs. To understand this, we need to investigate further and specifically study the flow field around pairs, not just the individual. The transitions in pair behavior across Reynolds numbers from in-line pairs to side-by-side pairs are in agreement with our initial hypothesis based on how the averaged flow field for an individual swimmer evolves with Re. We also see expected diverging (repulsive) behavior sideways switch to attractive behavior as Re increases. However, the transition to and formation of stable side-by-side pairs occurs at smaller Re, (2 for the V-pairs and 7 for the side-by-side orbits), compared to 15 for a single swimmer.

Moreover, we note that it is not obvious that five types of pairs would be stable nor that most initial configurations would give stable pairs. In fact, it could have been that a lot more initial configurations would result in the swimmers repelling and swimming away from one another, as seems to be the case for the 3D inertial squirmers, though fewer initial configurations were studied [49]. Of those initial configurations, Li $et\ al.$ found pushers which for Re < 5 would align along their swimming axis and form an in-line antiparallel pair. However, the swimmers afterwards rotated their swimming axes out of plane. They also identified pullers at Re = 10 which form a hydrodynamically entrapped pair with separate circular trajectories rotating in opposite directions, similar to the side-by-side orbit formed by dimers here but the dimers rotate together around their center of mass. Note that, as Re increases further Re > 25, we expect that a lot of the pairs will collide with higher velocities and more inertia and in return will become unstable, a behavior seen also in inertial squirmers.

Why do the inertial squirmers not form similar pairs? One big difference is that our model by construction allows for the full cycle of oscillation, which means that the swimmers interact hydrodynamically throughout the cycle and are free to rearrange. The compression and expansion throughout the cycle might be what allows swimmers to adjust
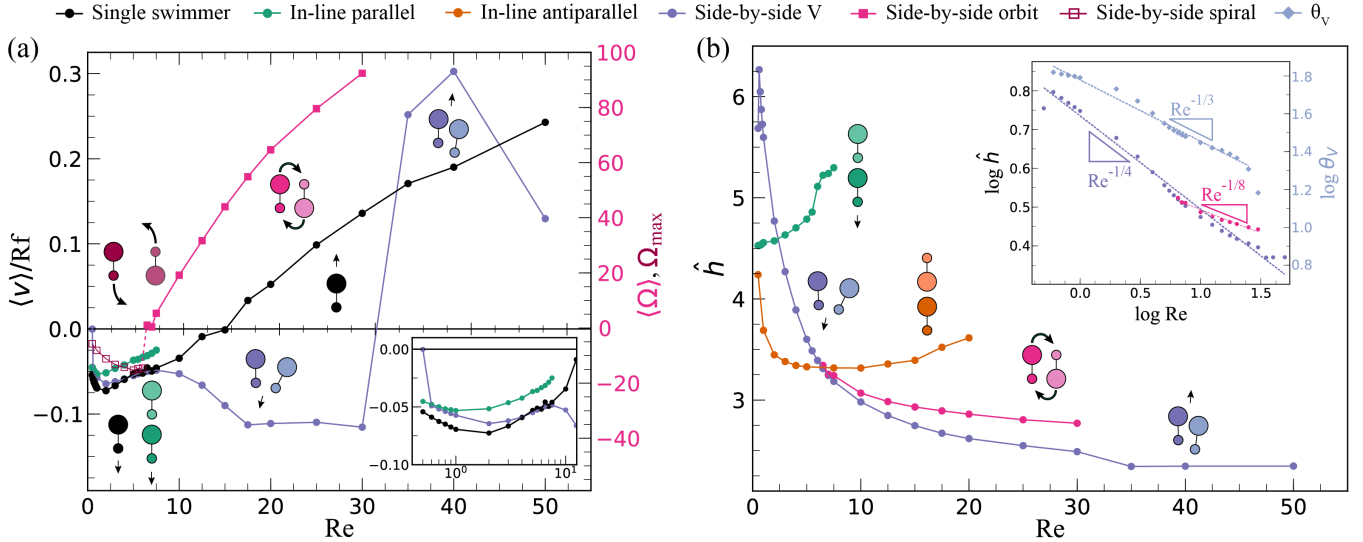
FIG. 5. (a) The swimming velocity of a side-by-side V pair (blue), a parallel in-line pair (green), and a single swimmer (black), as well as the angular velocity of the side-by-side orbit pair (pink) versus Re. The single swimmer switches its swimming direction from small-sphere-leading to large-sphere-leading at Re ≈ 15, the side-by-side V pair at Re ≈ 35 and the side-by-side orbit at Re ≈ 6.5. (b) The separation distance measured for the four stable pairs after they reached a steady state as a function of Re. The side-by-side pairs (pink and blue) separation monotonically decreases as Re increases, except for when Re = 0.5 for the V-shape pair. Here, the pair has formed an angle of 180 degrees with the small spheres closest. (b) inset: The separation distance for side-by-side pairs (pink and blue) as well as the angle between the two swimmers when they form a side-by-side V pair (black) plotted in log-log (base 10) values.

and coordinate their flows. In other words, it may not only be the average flow that matters. We should note that while the pairs can fit into these five categories where the details vary with Re, *e.g.* the angle between swimmers in the V-pair, the velocity at which the pair swims and their time-averaged fluid flows, as we discuss next.

To summarize, our main findings are the following. 1) There is a strong dependence on the initial configuration which is in agreement with previous work on Stokes and inertial squirmers [34, 49], and Stokes dimers [37–39]. 2) Unlike inertial squirmers, we find that for most initial conditions we actually assemble stable pairs. 3) Our stable pairs can be easily described and quantified into five categories. 4) There is a clear transition from in-line to side-by-side pairs as Re increases, as expected based on a transition of the flow field from puller-like (favors in-line) to pusher-like (favors side-by-side), but it is difficult to pinpoint the transition exactly. 5) The transition and formation of side-by-side pairs occurs at a smaller Re than expected from single-swimmer behavior. 6) The direction of swimming for the pair is not always the same as for the individual swimmer at the same Re.

D. Pair swim velocity, separation, and average fluid flows as a function of Re

We monitored the pairs' steady-state velocity, as well as the separation distance h across Re to understand how different pair dynamics compare to those of a single swimmer and thus provide insight into possible benefits behind each stable pair formation. We calculated the average velocity of the swimmers by averaging the velocity per oscillation over the total number of oscillations in steady state. For the orbit pair, we instead calculated the angular velocity in the same way. We excluded antiparallel in-line pairs from the comparison because they are stationary and have neither net translational nor angular velocity. A comparison of the velocities for the swimming and orbiting pairs and of a single swimmer are shown in Fig. 5(a) and the separation distance in Fig. 5(b). We also calculated the time-averaged fluid flow for the four stable pairs after they reached a steady state, over the range $0.5 \leq \text{Re} \leq 50$. We show these flows at four characteristic Reynolds numbers, Re = 0.5, 5, 20, and 35, that capture most of the interesting behavior, see Fig. 6(b-e). To allow for comparison between single and pair interactions, we also show the time-averaged fluid flow for a single swimmer at each Re, see Fig. 6(a). The way each pair was initialized is reported in the SI section IV [76]. We will discuss each pair separately and then compare between them.

1. Parallel in-line pair

The parallel in-line pair swims small-sphere-leading, and the velocity curve looks similar to the single swimmer in the Reynolds number range $0.5 \leq \mathrm{Re} \leq 7.5$, but with a slightly lower speed than the single swimmer case, see Fig. 5(a) green curve. Thus the presence of a second swimmer slows down the pair and can be attributed to an increase in the drag force. If we approximate one dimer swimmer as an ellipse, the aspect ratio would be ≈ 2.75. If we approximate the in-line pair of swimmers as a more elongated ellipse, the aspect ratio would be ≈ 5.5. Comparing the two, the drag force on the more elongated ellipse is larger [84, 85], which agrees with the reduction in speed we see in our data. In reality, for the pair, the swimmer in tow has less drag and bumps into the leading one. There may be benefits for swimmers to be in-line like this, but if so, it is not to increase pair speed. It may be, for example, to reduce the drag of the follower swimmers, which is known at high Re as seen in the V-formation of birds or humans cycling. What we show here is that it could be a factor in intermediate Re swimmers, too. For $\mathrm{Re} > 7.5$, the swimmers collide and push away from one another, so there is no stable pair for which to calculate an average translational velocity. While the speed of the pair is decreasing with increasing Re, the distance between the two swimmers increases, see Fig. 5(b). To understand why this happens, we look at the time-averaged fluid flows. As Re increases there is a gradual reversal of steady streaming flows from puller-like (pulling the in-line pair together), see Fig. 6(b.ii), to pusher-like (with flow pushing away along the swim direction, and pair axis direction) thus causing the two swimmers to move further apart. It seems that the development of the secondary outer vortex (steady streaming) around each swimmer that is responsible for the pusher flow makes them increase their distance, Fig. 2(b). The pair also switches from swimming small-sphere leading (down in Fig. 6(b.ii)) to large-sphere leading (up in (b.iii)). Eventually, the swimmers collide and diverge.

2. Antiparallel in-line pair

The antiparallel in-line pairs, as defined here with the large spheres closest, are generally stationary, but as Re increases they also undergo a transition in fluid flow and seem to remain stationary for different reasons at different Re. For the lowest Re's we studied, we see that the distance between the swimmers is quite large, yet they remain in the bound pair state. As Re increases, between $0.5 \leq \mathrm{Re} < 10$, the distance between the two swimmers drops, see Fig. 5(b) orange curve. Remember that at these low Re's each swimmer individually a) wants to swim in the direction of its small sphere, which, here, means breaking up the pair, and b) has a flow field around it that is pulling along its long axis. How do we explain this drop in the distance? One way to think about it is based on the boundary layer thickness which decreases as Re increases. That in itself allows the swimmers to be closer. We can see that in the two panels (c.i) and (c.ii) of Fig. 6, where the vorticity around the large spheres gets thinner as Re goes up resulting in a smaller separation distance. The swimmers seem to get trapped into a combined puller flow, forming a symmetric stationary pump Fig. 6(c.i)(c.ii) – which is surprising because if they acted as individual swimmers they would swim away from one another (small-sphere leading). It seems that the attractive strength between large spheres pulling the pair together is roughly equal to the forces generated by the swimming motion in the opposite direction (towards small spheres). As Re increases beyond 10, the flows reverse (Fig. 6(c.iii)(c.iv)) and now each swimmer wants to swim large-sphere-leading, resulting in the pair remaining stable, at first, with the swimmers bumping softly into one another. Eventually, they collide more strongly and diverge, which is indicated by an uptake in the distance between swimmers Fig. 5(b). The antiparallel in-line pair is essentially a stationary pump that prevents the swimmers from moving around. It could have benefits exactly for the same reason, such as mixing the fluid around it, or if we are interested in synthetic systems, the immobilization of motile particles.

3. V-pair

The V-pair occurs frequently and across all the Reynolds numbers we studied, though the exact details vary. Consider the V-pair velocity and fluid flow as a function of Re, Figs. 5(a) blue curve and 6(d). At $\mathrm{Re} = 0.5$ the pair is immotile, its velocity is zero and acts like a pump. The angle between the swimmers, at this low Re, is 180 degrees, meaning that the pair forms a line with their small spheres closest. We could have considered this a separate case, but it seems that as Re increases, the angle decreases monotonically (Fig. 5(b) inset) corresponding to a V-shape, so we considered it as such. From $0.5 < \mathrm{Re} \leq 7.5$ the V-pair and the single swimmer's velocity curves are close to identical. The flow field around the pair for $\mathrm{Re} = 5$ is qualitatively different from the puller-like flow field around a single swimmer at the same Re, see Figs. 6(d.ii) and (a.ii) respectively. Specifically, the flow field for the pair at $\mathrm{Re} = 5$ pulls in along the swimming axis from underneath the small spheres, pulls through the pair like a zipline, and pushes out behind the large spheres, while elongated vortices return the flow back towards the small spheres.

The single swimmer on the other hand looks like a puller. Yet, the pair and single swimmer are similar both in the direction of swimming and their speed, which is surprising. The distance between swimmers and the angle both monotonically decrease as Re increases. This can also be seen visually by looking at the averaged fluid flows as a function of Re Fig. 6(d).

Looking at the velocity curves of the V-pair versus the single swimmer we see that for Re > 7.5 they diverge. The V-pair actually speeds up till it stops moving in a straight line, picks up a rotational velocity, and moves on an arc (which is probably the reason for the plateau of the translational velocity around Re ≈ 17, see Fig. 5(a)). Nonetheless, it seems that the V-pair swims faster than the individual in the Re range roughly between $10 - 20$. At Re $= 20$, the flow field of the pair resembles a pusher though the field is not quite as symmetric as in the single swimmer case (also pusher-like), see Fig. 6(d.iii) and (a.iii), or as in the V-pair at lower Re.

At Re ≈ 35, we see a sharp transition where the swim direction switches from small-sphere-leading to large-sphere-leading. In other words, the Reynolds number at which the switch in swim direction occurs is much larger for the pair (Re $= 35$) than for the single swimmer (Re ≈ 15), which was not predicted. Looking closely, the switch in swimming direction for the V-pair coincides with a change in the swim stroke. The pair staggers, switches leading swimmers, and sheds vortices, Fig. 6(d.iv). For a more dynamic visualization, see the movie provided in the SI section V, movie S3 [76]. When Re > 50 swimmers physically collide and no longer form a stable pair. It is possible that there is a Re for which the V-pair's trajectory starts to form an arc, and that there a dependence with Re as Re increases further. However, it is difficult to evaluate here because of the size of the box and the fact that the pair becomes unstable at high Re.

At this point, it is useful to discuss the scaling of the distance between the swimmers of a V-pair, where there is an interesting connection to granular systems. In previous works, we showed that an externally vibrated system of spherical grains assembles pairs and chains (if there are many particles) perpendicular to the direction of the oscillation, driven by steady streaming flows [82, 83]. The particles in the pair aligned perpendicular to the direction of oscillation, adjusted to sit at a well-defined distance and oscillated in phase. The preferred distance was empirically (experiments and simulations) found to have two scalings depending on the Re: δ^2/d for Re < 50 and $\delta A/d$ for Re > 50, where δ is the oscillatory boundary layer thickness, d is the particle diameter and A is the amplitude of the particle with respect to the fluid. Note that for a single sphere, the stagnation point between the inner and outer streaming flows also scales as δ^2/d [86]. So, how (if so) does the scaling of the swimmers that form a V-pair relate to the externally-vibrated granular case? The scaling of the distance for the V-pair is $\sim 1/(\text{Re})^{\frac{1}{4}} = \frac{\delta^{1/2}}{rA_r}$ which is a faster decay compared to the granular system of two spheres.

4. Orbit pair

For Re < 6.5 the swimmers swim small-sphere-leading and move away from one another in a spiral, see Fig. 6(e.i, e.ii) and SI section V, movie S4 [76]. The side-by-side orbit pair is stable for Re ≥ 6.5 and the pair always orbits in the direction of the large spheres, see Fig. 6(e.iii). The angular velocity of the stable orbit pair increases monotonically with increasing Re, see Fig. 5(a) pink curve. We see that having two interacting swimmers instead of a single one changes the dynamics: while the single swimmer transitions from small-sphere-leading to large-sphere-leading at Re ≈ 15, the orbiting pair makes an analogous transition from a small-sphere-leading diverging spiral to a large-sphere-leading stable orbit at a lower Re ≈ 6.5. As Re increases (*e.g.* Re $= 20$), the flows become more complex, see Fig. 6(e.iii) and movie S6 in the SI section V [76]. The distance between the two swimmers decreases monotonically (similarly to the V-pair).

For Re > 30, the swimmers physically collide and are unable to maintain a stable orbit, see Fig. 6(e.iv). It is interesting to note that the orbit introduces an additional length scale $(\frac{\nu}{\Omega})^{1/2}$ where Ω is the angular velocity of the orbit, see for example the spontaneous orbiting of a granular dimer [87].

IV. CONCLUSIONS

We computationally studied the behavior of asymmetric, dimer swimmer pairs over a range of intermediate Reynolds numbers and initial configurations. We found the emergence of five assembled stable pairs both stationary and motile, arranged in-line and side-by-side (parallel and anti-parallel), and perpendicular. The stable pairs have motility characteristics (time-averaged fluid flows, swim speeds) that in some cases are simple extensions of the single swimmer, while in other cases we found novel states, such as the orbit, and the immotile pump. A general trend we see as Re increases is a transition from in-line pairs (at low Re) to side-by-side pairs (at high Re). The trend seems to be correlated to the time-averaged fluid flows around the single swimmer, *i.e.* steady streaming, that transition from puller-like (favoring in-line pairs) to pusher-like (favoring side-by-side pairs). For the motile pairs, we compared
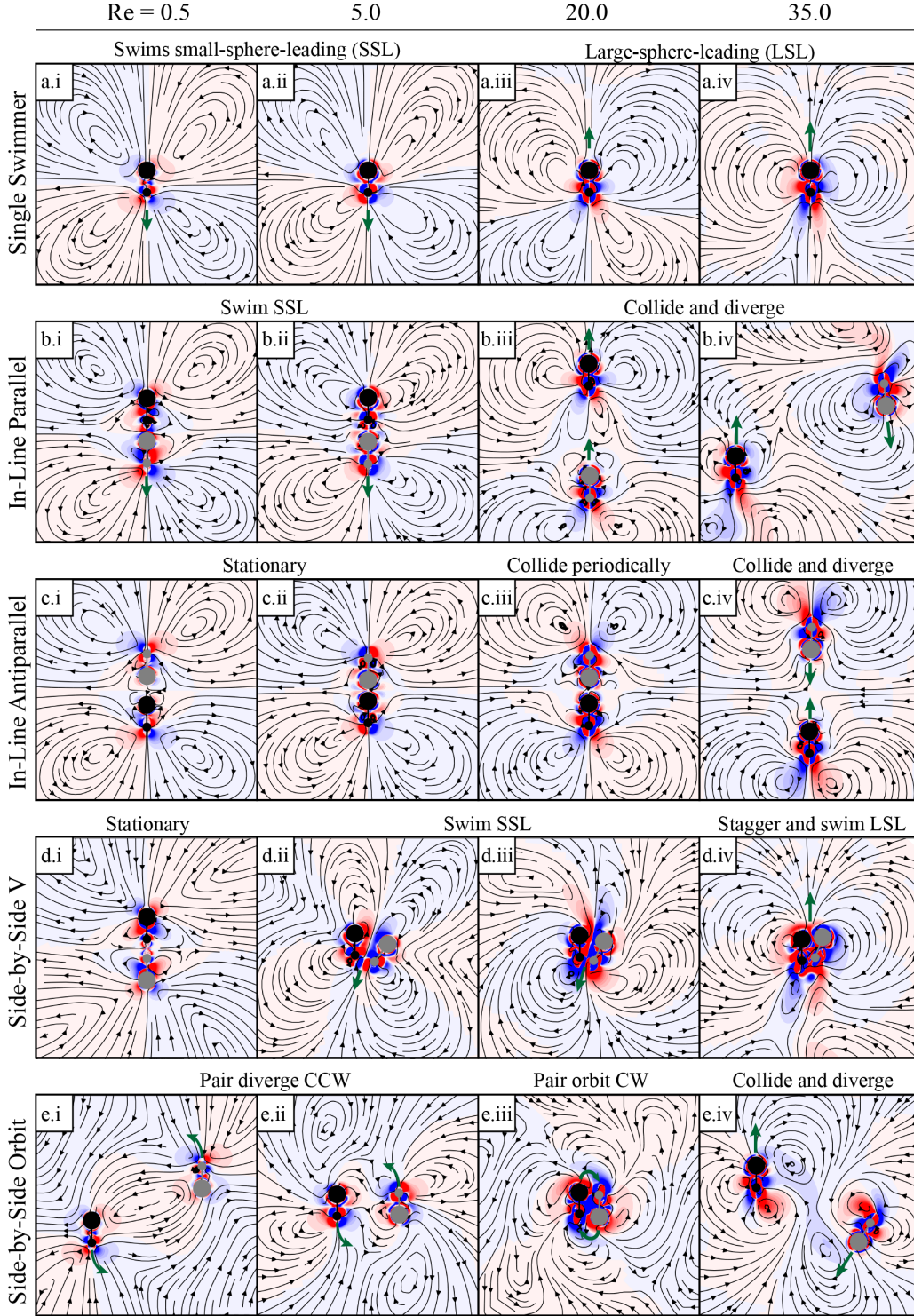
FIG. 6. Time-averaged fluid flow for (a) an individual dimer, and pairs that are (b) in-line parallel, (c) in-line anti-parallel, (d) side-by-side V-shapes, and (e) side-by-side orbits, on the 100th swim stroke, $\tau = 100$. Individual swimmer flow and swim direction transitions from puller-like small-sphere-leading (a.i, a.ii) to pusher-like large-sphere-leading (a.iii, a.iv). (b) Parallel in-line pairs form when Re < 10 and diverge otherwise. (c) Anti-parallel in-line pairs transition from stationary pumps to swimmers in a periodically occurring head-on collision. (d) Side-by-side configurations form a stationary pump pair, a V-shape which swims in the direction of the small sphere, and a staggering V-shape which swims in the direction of the large sphere. (e) Side-by-side orbits diverge swimming in the direction of the small sphere when Re < 6.5, and form a stable orbit that rotates in the direction of the large spheres when $6.5 \leq \text{Re} < 30$. The heatmap is color coded by vorticity where red represents a counter-clockwise rotation and blue a clockwise rotation.

their swim speeds, swim direction and fluid flows to those of the single swimmer. The in-line pairs, that are more frequent at the low end of Re, resembled an elongated single swimmer if arranged in parallel and an immotile pump if arranged antiparallel. There were no stable in-line pairs at higher Re's. In contrast, for the side-by-side pairs we discovered differences compared with the single swimmer behavior: the critical Reynolds number where the swim direction switched was lower than the single swimmer's for the orbit, and larger for the V-pair; the time-averaged fluid flow directions were also more complex for these pairs. We expect the interactions and assemblies discussed here to be present in various biological systems at these scales, and to be relevant for artificial and robotic ones.

From a materials point of view, our findings provide a guide to self-assembling different pair configurations through systematic design, by careful tweaking of the fluid inertia and can be used as the basis for scaling up towards many-body interactions. Specifically, our results in Fig.4 can be a useful tool for assembly prediction, because it seems that knowing the average flow field and direction of swimming for a single swimmer, and the initial positions and orientations for the pair, one can make a good estimate as to which of the five stable pairs will form: it is the stable pair that is geometrically the closest to the initial positions, taking into account the flow field and direction of swimming for the single swimmer.

The fact that the swim direction transitions between small-sphere-leading to large-sphere-leading at different Res for each stable pair and compared to the single swimmer (Fig.5(a)), the different speeds and shape of the velocity curves as a function of Re, and the formation of immotile pumps and orbits are interesting results that lead to several insights. For example, they indicate that coordinated swimmers in pairs may be hydrodynamically beneficial (faster) versus isolated swimming. In other cases, coordinated swimming in pairs is slower and that may be beneficial for overall energy saving *e.g.* in biological organisms. In the future, it would be interesting to determine specifically possible advantages behind forming stable pairs or multiple-swimmer assemblies versus isolated swimming, *e.g.* by measuring and comparing efficiencies, and stresses, and to be able to connect to experiments. Moreover, our results suggest that an effective Reynolds number (or other dimensionless ratio) which accounts for the number of swimmers might be a useful tool for describing many-body systems, as has been discussed for Stokes swimmers [88] and for inertial swimmers [52]. Our analytical results, reported recently for the single dimer swimmer, show that the motility behavior is sensitive to the balance between the finite inertia of the swimmer and of the fluid [70]. It is perhaps then no surprise that when a second swimmer is introduced, the interactions become a lot more complicating and more interesting.

The pairwise or collective behavior of real systems, biological or artificial, at intermediate Re has hardly been studied especially from a physics perspective. In our simple model, the fluid interactions between the swimmers lead to assemblies of dynamic pairs that are either swimming together, constituting a first step towards flocking, or together canceling each other becoming essentially stationary immotile pumps or orbits. Building on these pairwise interactions and systems like the ones presented here is a way to to test ideas and glean intuition in order to formulate a statistical mechanics framework for inertial suspensions, as presented for example by Chaterjee *et al.* [52], and open up the field to explore more systems of active matter on the mesoscale [59].

---

[1] J. Krause, G. D. Ruxton, and S. Krause, Swarm intelligence in animals and humans, Trends Ecol. Evol. **25**, 28 (2010).

[2] T. Vicsekand A. Zafeiris, Collective motion, Physics Reports **517**, 71 (2012), collective motion.

[3] M. C. Marchetti, J. F. Joanny, S. Ramaswamy, T. B. Liverpool, J. Prost, M. Rao, and R. A. Simha, Hydrodynamics of soft active matter, Reviews of Modern Physics **85**, 1143 (2013).

[4] J. Dunkel, S. Heidenreich, K. Drescher, H. H. Wensink, M. Bär, and R. E. Goldstein, Fluid dynamics of bacterial turbulence, Physical review letters **110**, 228102 (2013).

[5] M. E. Catesand J. Tailleur, Motility-Induced Phase Separation, Annual Review of Condensed Matter Physics **6**, 219 (2015).

[6] S. C. Takatoriand J. F. Brady, Forces, stresses and the (thermo?) dynamics of active matter, Current Opinion in Colloid & Interface Science **21**, 24 (2016).

[7] S. Ramaswamy, Active matter, Journal of Statistical Mechanics: Theory and Experiment , 054002 (2017).

[8] D. Needlemanand Z. Dogic, Active matter at the interface between materials science and cell biology, Nature Reviews Materials **2**, 28 (2017).

[9] N. T. Ouellette, The most active matter of all, Matter **1**, 297 (2019).

[10] M. Rubenstein, A. Cornejo, and R. Nagpal, Programmable self-assembly in a thousand-robot swarm, Science **345** (2014).

[11] G.-Z. Yang, J. Bellingham, P. E. Dupont, P. Fischer, L. Floridi, R. Full, N. Jacobstein, V. Kumar, M. Mc-Nutt, R. Merrifield, B. J. Nelson, B. Scassellati, M. Taddeo, R. Taylor, M. Veloso, Z. L. Wang, and R. Wood, The grand challenges of science robotics, Science Robotics **3**, 10.1126/scirobotics.aar7650 (2018), https://robotics.sciencemag.org/content/3/14/eaar7650.full.pdf.

[12] A. Ghosh, W. Xu, N. Gupta, and D. H. Gracias, Active matter therapeutics, Nano Today **31**, 100836 (2020).

[13] A. De Rosis, E. Lévêque, S. Ubertini, and Succi, Spread of consensus in self-organized groups of individuals: Hydrodynamics matters, EPL (Europhysics Letters) **113**, 18001 (2016).

[14] E. M. Purcell, Life at low Reynolds number, American Journal of Physics **45**, 3 (1977).

[15] E. Laugaand T. R. Powers, The hydrodynamics of swimming microorganisms, Reports on Progress in Physics **72**, 096601 (2009).

[16] A. Najafiand R. Golestanian, Simple swimmer at low Reynolds number: Three linked spheres, Physical Review E **69**, 062901 (2004).

[17] P. Satirand M. A. Sleigh, The physiology of cilia and mucociliary interactions, Annual review of physiology **52**, 137 (1990).

[18] C. Brennenand H. Winet, Fluid mechanics of propulsion by cilia and flagella, Annual Review of Fluid Mechanics **9**, 339 (1977).

[19] E. Lauga, Continuous breakdown of purcell's scallop theorem with inertia, Physics of Fluids **19**, 061703 (2007).

[20] N. G. Chisholm, D. Legendre, E. Lauga, and A. S. Khair, A squirmer across reynolds numbers, Journal of Fluid Mechanics **796**, 233 (2016).

[21] M. J. McHenry, E. Azizi, and J. A. Strother, The hydrodynamics of locomotion at intermediate Reynolds numbers: undulatory swimming in ascidian larvae (Botrylloides sp.), Journal of Experimental Biology **206**, 327 (2003).

[22] G. Herschlagand L. Miller, Reynolds number limits for jet propulsion: a numerical study of simplified jellyfish, Journal of theoretical biology **285**, 84 (2011).

[23] S. Childress, *Mechanics of swimming and flying* (Cambridge University Press, 1981).

[24] S. Vogel, *Life's devices: the physical world of animals and plants* (Princeton University Press, 1988).

[25] D. L. Kochand G. Subramanian, Collective hydrodynamics of swimming microorganisms: Living fluids, Annual Review of Fluid Mechanics **43**, 637 (2011), https://doi.org/10.1146/annurev-fluid-121108-145434.

[26] H. Xu, J. Dauparas, D. Das, E. Lauga, and Y. Wu, Self-organization of swimmers drives long-range fluid transport in bacterial colonies, Nature communications **10**, 1 (2019).

[27] J. Koiller, K. Ehlers, and R. Montgomery, Problems and progress in microswimming, Journal of Nonlinear Science **6**, 507 (1996).

[28] S. Gueronand K. Levit-Gurevich, Energetic considerations of ciliary beating and the advantage of metachronal coordination, Proceedings of the National Academy of Sciences **96**, 12240 (1999).

[29] S. Granzier-nakajima, R. D. Guy, and C. Zhang-molina, A Numerical Study of Metachronal Propulsion at Low to Intermediate Reynolds Numbers, Fluids , 86 (2020).

[30] H. Nguyenand D. Klotsa, Nonreciprocal model swimmer at intermediate reynolds numbers, arXiv:2108.00095 (2022).

[31] A. Sokolov, S. Zhou, O. D. Lavrentovich, and I. S. Aranson, Individual behavior and pairwise interactions between microswimmers in anisotropic liquid, Physical Review E **91**, 013009 (2015).

[32] G. J. Elfringand E. Lauga, Passive hydrodynamic synchronization of two-dimensional swimming cells, Physics of Fluids **23**, 011902 (2011).

[33] Y. Yang, J. Elgeti, and G. Gompper, Cooperation of sperm in two dimensions: synchronization, attraction, and aggregation through hydrodynamic interactions, Physical review E **78**, 061903 (2008).

[34] T. Ishikawa, M. Simmonds, and T. J. Pedley, Hydrodynamic interaction of two swimming model micro-organisms, Journal of Fluid Mechanics **568**, 119 (2006).

[35] A. Kanevsky, M. J. Shelley, and A.-K. Tornberg, Modeling simple locomotors in stokes flow, Journal of Computational Physics **229**, 958 (2010).

[36] K. Lippera, M. Benzaquen, and S. Michelin, Bouncing, chasing, or pausing: Asymmetric collisions of active droplets, Physical Review Fluids **5**, 032201 (2020).

[37] G. Alexanderand J. Yeomans, Dumb-bell swimmers, EPL (Europhysics Letters) **83**, 34006 (2008).

[38] E. Laugaand D. Bartolo, No many-scallop theorem: Collective locomotion of reciprocal swimmers, Physical Review E **78**, 030901 (2008).

[39] V. B. Putzand J. Dunkel, Low Reynolds number hydrodynamics of asymmetric, oscillating dumbbell pairs, The European Physical Journal Special Topics **187**, 135 (2010).

[40] T. Y. Wu, Fish swimming and bird/insect flight, Annual Review of Fluid Mechanics **43**, 25 (2011), https://doi.org/10.1146/annurev-fluid-122109-160648.

[41] C. Hemelrijk, D. Reid, H. Hildenbrandt, and J. T. Padding, The increased efficiency of fish swimming in a school, Fish and Fisheries **16**, 511 (2015).

[42] A. D. Becker, N. Masoud, Hassan, J. W., M. Shelley, and L. Ristroph, Hydrodynamic schooling of flapping swimmers, Nature Communications **6**, 10.1038/ncomms9514 (2015).

[43] M. Daghooghiand I. Borazjani, The hydrodynamic advantages of synchronized swimming in a rectangular pattern, Bioinspiration & Biomimetics **10**, 056018 (2015).

[44] M. Gazzola, A. Tchieu, D. Alexeev, A. de Brauer, and P. Koumoutsakos, Learning to school in the presence of hydrodynamic interactions, Journal of Fluid Mechanics **789**, 726 (2016).

[45] A. P. Maertens, A. Gao, and M. S. Triantafyllou, Optimal undulatory swimming for a single fish-like body and for a pair of interacting swimmers, Journal of Fluid Mechanics **813**, 301 (2017).

[46] J. W. Newbolt, J. Zhang, and L. Ristroph, Flow interactions between uncoordinated flapping swimmers give rise to group cohesion, Proceedings of the National Academy of Sciences **116**, 2419 (2019), https://www.pnas.org/content/116/7/2419.full.pdf.

[47] K. Lippera, M. Benzaquen, and S. Michelin, Alignment and scattering of colliding active droplets, Soft Matter **17**, 365 (2021).

[48] I. O. Götzeand G. Gompper, Mesoscale simulations of hydrodynamic squirmer interactions, Physical Review E **82**, 041921 (2010).

[49] G. Li, A. Ostace, and A. M. Ardekani, Hydrodynamic interaction of swimming organisms in an inertial regime, Physical Review E **94**, 053104 (2016).

[50] S. Alben, Collective locomotion of two-dimensional lattices of flapping plates. part 1. numerical method, single-plate case and lattice input power, Journal of Fluid Mechanics **915**, A20 (2021).

[51] S. Alben, Collective locomotion of two-dimensional lattices of flapping plates. part 2. lattice flows and propulsive efficiency, Journal of Fluid Mechanics **915**, A21 (2021).

[52] R. Chatterjee, N. Rana, R. A. Simha, P. Perlekar, and S. Ramaswamy, Inertia drives a flocking phase transition in viscous active fluids, Phys. Rev. X **11**, 031063 (2021).

[53] R. Ouillon, I. A. Houghton, J. O. Dabiri, and E. Meiburg, Active swimmers interacting with stratified fluids during collective vertical migration, Journal of Fluid Mechanics **902**, A23 (2020).

[54] E. Kunze, J. F. Dower, I. Beveridge, R. Dewey, and K. P. Bartlett, Observations of biologically generated turbulence in a coastal inlet, Science **313**, 1768 (2006).

[55] M. M. Wilhelmusand J. O. Dabiri, Observations of large-scale fluid transport by laser-guided plankton aggregations a), Physics of Fluids **26**, 101302 (2014).

[56] J. C. Nawrothand J. O. Dabiri, Induced drift by a self-propelled swimmer at intermediate Reynolds numbers, Physics of Fluids **26**, Art (2014).

[57] I. A. Houghton, J. R. Koseff, S. G. Monismith, and J. O. Dabiri, Vertically migrating swimmers generate aggregation-scale eddies in a stratified column, Nature **556**, 497 (2018).

[58] N. G. Chisholmand A. S. Khair, Partial drift volume due to a self-propelled swimmer, Physical Review Fluids **3**, 014501 (2018).

[59] D. Klotsa, As above, so below, and also in between: mesoscale active matter in fluids, Soft matter **15**, 8946 (2019).

[60] D. Klotsa, K. A. Baldwin, R. J. A. Hill, R. M. Bowley, and M. R. Swift, Propulsion of a Two-Sphere Swimmer, Phys. Rev. Lett. **115**, 248102 (2015).

[61] B. U. Felderhof, Effect of fluid inertia on the motion of a collinear swimmer, Physical Review E **94**, 063114 (2016).

[62] J. F. Collis, D. Chakraborty, and J. E. Sader, Autonomous propulsion of nanorods trapped in an acoustic field, Journal of Fluid Mechanics **825**, 29 (2017).

[63] T. Dombrowski, S. K. Jones, G. Katsikis, A. P. S. Bhalla, B. E. Griffith, and D. Klotsa, Transition in swimming direction in a model self-propelled inertial swimmer, Physical Review Fluids **4**, 021101 (2019).

[64] T. Parthasarathy, F. K. Chan, and M. Gazzola, Streaming-enhanced flow-mediated transport, Journal of Fluid Mechanics **878**, 647 (2019).

[65] J. A. Puente-Velzquez, F. A. Godnez, E. Lauga, and R. Zenit, Viscoelastic propulsion of a rotating dumbbell, Microfluidics and Nanofluidics **23**, 108 (2019).

[66] T. Dombrowskiand D. Klotsa, Kinematics of a simple reciprocal model swimmer at intermediate reynolds numbers, Physical Review Fluids **5**, 063103 (2020).

[67] B. U. Felderhof, Collinear velocity relaxation of two spheres in a viscous incompressible fluid, Physical Review E **101**, 043103 (2020).

[68] M. Hubert, O. Trosman, Y. Collard, A. Sukhov, J. Harting, N. Vandewalle, and A.-S. Smith, Scallop theorem and swimming at the mesoscale, Physical Review Letters **126**, 224501 (2021).

[69] J. P. Binagiaand E. S. G. Shaqfeh, Self-propulsion of a freely suspended swimmer by a swirling tail in a viscoelastic fluid, Physical Review Fluids **6**, 053301 (2021).

[70] N. J. Derr, T. Dombrowski, C. H. Rycroft, and D. Klotsa, Fluid inertia and the scallop theorem, arXiv preprint arXiv:2202.03669 (2022).

[71] G. S. Klindtand B. M. Friedrich, Flagellar swimmers oscillate between pusher- and puller-type swimming, Physical Review E **92**, 063019 (2015).

[72] B. E. Griffith, R. D. Hornung, D. M. McQueen, and C. S. Peskin, An adaptive, formally second order accurate version of the immersed boundary method, Journal of Computational Physics **223**, 10 (2007).

[73] B. E. Griffith, Immersed boundary model of aortic heart valve dynamics with physiological driving and loading conditions, International Journal for Numerical Methods in Biomedical Engineering **28**, 317 (2012).

[74] B. Kallemov, A. P. S. Bhalla, B. E. Griffith, and A. Donev, An immersed boundary method for rigid bodies, Comm Appl Math Comput Sci **11**, 79 (2016).

[75] F. Balboa Usabiaga, B. Kallemov, B. Delmotte, A. P. S. Bhalla, B. E. Griffith, and A. Donev, Hydrodynamics of suspensions of passive and active rigid particles: a rigid multiblob approach, Communications in Applied Mathematics and Computational Science **11**, 217 (2016).

[76] See Supplementary Information for more details on methods, additional figures and movies.

[77] B. E. Griffith, X. Luo, D. M. McQueen, and C. S. Peskin, Simulating the fluid dynamics of natural and prosthetic heart valves using the immersed boundary method, Int. J. Appl. Mech. **1**, 137 (2009).

[78] N. Riley, Steady streaming, Annual Review of Fluid Mechanics **33**, 43 (2001).

[79] N. Riley, On a sphere oscillating in a viscous fluid, Quart. Journ. Mech. and Applied Math **XIX**, 461 (1966).

[80] N. Riley, The steady streaming induced by a vibrating cylinder, J. Fluid Mech. **68**, 801 (1975).

[81] W. Coenenand N. Riley, Oscillatory flow about a cylinder pair, The Quarterly Journal of Mechanics and Applied Mathematics **62**, 53 (2009), https://academic.oup.com/qjmam/article-pdf/62/1/53/5305586/hbn024.pdf.

[82] D. Klotsa, M. R. Swift, R. M. Bowley, and P. J. King, Interaction of spheres in oscillatory fluid flows, Phys. Rev. E **76**, 056314 (2007).

[83] D. Klotsa, M. R. Swift, R. M. Bowley, and P. J. King, Chain formation of spheres in oscillatory fluid flows, Phys. Rev. E **79**, 021302 (2009).

[84] R. Ouchene, M. Khalij, A. Taniasre, and B. Arcen, Drag, lift and torque coefficients for ellipsoidal particles: From low to moderate particle reynolds numbers, Computers and Fluids **113**, 53 (2015), small scale simulation of multiphase flows.

[85] S. K. Sanjeevi, J. Kuipers, and J. T. Padding, Drag, lift and torque correlations for non-spherical particles from stokes limit to high reynolds numbers, International Journal of Multiphase Flow **106**, 325 (2018).

[86] C. W. Kotas, M. Yoda, and P. H. Rogers, Visualization of steady streaming near oscillating spheroids, Experiments in fluids **42**, 111 (2007).

[87] H. A. Pacheco-Martinez, L. Liao, R. J. A. Hill, M. R. Swift, and R. M. Bowley, Spontaneous orbiting of two spheres levitated in a vibrated liquid, Phys. Rev. Lett. **110**, 154501 (2013).

[88] L. H. Cisneros, R. Cortez, C. Dombrowski, R. E. Goldstein, and J. O. Kessler, Fluid dynamics of self-propelled microorganisms, from individuals to concentrated populations, Experiments in Fluids **43**, 737 (2007).